Three-body continuum energy correlations in Borromean halo nuclei. II

B. V. Danilin,[1,*] J. S. Vaagen,[1] T. Rogde,[1] S. N. Ershov,[1,†] I. J. Thompson,[2] and M. V. Zhukov[3]

[Russian-Nordic-British Theory (RNBT) Collaboration]

[1]*Department of Physics and Technology, University of Bergen, Norway*
[2]*Physics Department, University of Surrey, Guildford, Surrey, GU2 7XH, United Kingdom*
[3]*Fundamental Physics, Chalmers University of Technology, S-41296 Göteborg, Sweden*

The general properties of intrinsic energy correlations in the three-body continuum of Borromean halo nuclei are considered. A model that describes the system as a three-body $\alpha + n + n$ cluster structure and reproduces the experimentally known properties of ^{6}He and ^{6}Li is used to study low-lying resonances and soft modes. The intrinsic correlated structure of the ^{6}He continuum reveals a unique structure for three-body 2_1^+, 2_2^+, and 1_1^+ resonances and a lack of resonant structure in soft dipole and monopole modes.

I. INTRODUCTION

Developments during the past decade of dynamic approaches to three-body continuum theory [1–4] have made it possible to perform detailed studies of specific features of the continuum of a Borromean system with a halo ground state. This article continues our studies of the continuum properties of halo nuclei, with particular reference to and illustrations for ^{6}He. Three-body $\alpha + n + n$ dynamics, determined by the three-body Schrödinger equation within the method of hyperspherical harmonics (HH) (see Refs. [1,2,5,6]) has by now been consistently applied for both bound and continuum states. A "realistic" αn interaction [5] with purely repulsive s-wave component and the GPT nn interaction [7] were used, reproducing resonances and phase shifts in the binary channels. In our articles [1,2] we have investigated three-body scattering phase shifts and simple responses of transitions from halo ground state to the continuum, summed over final states. We found a significant compression of the low-lying continuum spectrum for ^{6}He, compared to calculations where all binary potentials were progressively increased by scaling factors $\lambda > 1$ to make structures and states bound.

For three-body Borromean systems, an ideal experiment would be to observe the intrinsic structure of the continuum in $3 \rightarrow 3$ scattering, but such experiments seem impossible at present to perform in the laboratory. Thus, we have to be satisfied with more or less complicated reactions that induce transitions from the halo ground state (g.s.) to the three-body continuum. One-step reaction theories [for example DWBA, or the semiclassical electromagnetic dissociation (EMD) method] intertwine correlations from both the g.s. and the three-body continuum, with additional distortion from reaction mechanisms. We will return to this topic in a forthcoming

paper, so in the present paper, even if $3 \rightarrow 3$ scattering remains a thought experiment, we study the genuine intrinsic features of the Borromean continuum theoretically.

The doubly peaked ("di-neutron"+"cigar") plot [5,6] for the spatial correlation density of the ^{6}He g.s. has been a useful tool for elucidating halo properties. Recently, in Ref. [8] (henceforth referenced as (I)) we have calculated similar spatial correlation densities of the continuum wave functions in ^{6}He. By summing over angles and partial waves, plots of the continuum correlated densities were presented in coordinate space. The present paper continues this analysis and discusses the physics contained in intrinsic *energy correlations* of the three-body continuum.

The three-body dynamics has previously been successfully tested in calculations for bound and lowest excited states of the $A = 6$ nuclei [1,5], for calculation of the dipole strength function [9], and inelastic ^{6}He(n, n') and charge-exchange ^{6}Li(n, p) reactions to the ^{6}He continuum [4,10]. The continuum and g.s. wave functions were more recently also used for studying elastic and inelastic breakup of ^{6}He on ^{12}C and Pb targets [11] under the kinematically complete conditions of GSI experiments [12]. Very recently [13], angular and energy correlations have been measured and compared with predictions of our models [2].

The three-body continuum structure of ^{6}He, which we have used as a reference case for more complicated halo nuclei, exhibits a challenging structure. In addition to the sharp 2_1^+ three-body resonance at 0.8 MeV above the three-body threshold, a second 2_2^+ resonance has been calculated at an energy of 2.1 MeV with a width $\Gamma \simeq 1.4$ MeV, a 1^+ resonance at $E = 2$ MeV with $\Gamma \cong 1.2$ MeV, and a 0^+ excitation peaking at $E = 1.6$ MeV with $\Gamma = 1.5$ MeV. Evidence for the three-body resonance behavior has been derived both from well-defined potential pockets and from scattering eigenphases.

A question that has not yet been fully answered after more than a decade is that of the origin of accumulation of dipole strength at low continuum energy. The nature of the so-called soft dipole mode, suggested in [14], and responsible for the abnormally large EMD cross sections, still needs clarification

---

*Permanent address: Russian Research Center "The Kurchatov Institute," 123182 Moscow, Russia.

†Permanent address: Joint Institute for Nuclear Research, 141980 Dubna, Russia.

and is of great interest for theory as it involves both *s* and *p* motion [15,16] of valence neutrons.

Various attempts [1,2,9,17–26], based on the three-body representation of ^{6}He and ^{11}Li, have not given a conclusive answer concerning the existence of a dipole resonance in either ^{6}He or ^{11}Li. For example, neither the most elaborated methods such as HH with strict treatment of the three-body continuum [1,2,9], nor the complex rotation method applied to the three-body Schrödinger equation [20,25,27], nor the three-body RGM [17] show the dipole mode as resonance. At the same time, in the adiabatic hyperspherical approach, in particular using the complex energy (Gamow states) method, numerous resonant poles were calculated by the Aarhus group [23] in the ^{6}He dipole continuum.

Available experimental results, where the dipole response function of ^{6}He in EMD is reconstructed [12], do not show the 1- to 2-MeV sharp peak in the dipole strength function predicted by some three-body approaches but is consistent with our findings [28].

Given these considerations, it is possible to point out four main sources of enhancements of the continuum cross sections:

(i) true three-body resonances, which are caused by interaction of *all three* particles in the interior domain;
(ii) a long-lived binary resonance in one of the constituent pairs;
(iii) resonances resulting from strong coupling between channels (a "CC resonance" in a few channels) or "parametric resonance" in quantum diffusion with complex coefficients [29,30]; and
(iv) The low-energy response of an extended system (having a halo-like g.s. structure) to long-range transition operators used to excite the continuum.

The resonance criteria are similar to those in the two-body case: (a) a concentration of the wave function in the interior region (except for barrier top and virtual-state or antibound cases), and (b) that the existence and properties of an intrinsic resonant state should *not* depend on the reaction mechanism (electromagnetic, strong or weak interaction, etc.) that excites the resonance. In the three-body halo problem, we have however to deal with "binary" subsystems, involving any pair of particles and the relative motion of this pair with respect to the third constituent. Thus we should analyze correlation properties of three-body system to clarify the sometimes complicated structure of the continuum.

In the current article, we analyze the continuum wave functions in terms of their asymptotic amplitudes and elastic cross sections when written as functions of the *energies* of the pairs of Jacobi coordinates. We give an analysis of two-dimensional intrinsic energy correlations in a Borromean three-body problem, pointing out their simplest analytical properties and possibilities thereby for discriminating experimental and/or theoretical ambiguities.

We use, as already mentioned, realistic potentials for the ^{6}He benchmark case [1–3,7] and the Feshbach reduction method for reducing a nearly complete functional space (up to hyperangular momentum $K \sim 40$ for high-accuracy convergence) to an active space of $K \leqslant 11$ [11] giving the

same values for a wide set of the bound-state and continuum observables.

II. THEORETICAL OVERVIEW

A. Three-body dynamics

The three-body *continuum* problem includes two extreme scales of three-body effective interactions [8]:

(i) A short-range scale with a size about the sum of the ranges of the binary interactions, which produces compact spatial structure such as a true three-body resonance. The most remarkable feature of a "true" three-body resonance is that it exists in the configurations with the lowest hyperangular momenta (hypermoments), which corresponds to all three particles interacting while close to each other.
(ii) The phenomenon of a long-ranged effective three-body interaction with a range about the sum of the *scattering lengths* in the binary subsystems. This is responsible for the Efimov effect [31] and for spectral compression near the three-body threshold in Borromean halo nuclei.

In general (b) reflects the presence of the interaction between a particle pair and a third constituent even at a distance up to the scattering length. For short-range binary interactions, the effective three-body interaction (the angular-spin-projected sum of three binary interactions) is a function $V(\rho)$ of a collective variable, the hyperradius ρ, with characteristic asymptotic behavior $\sim 1/\rho^3$ in the general case, and $\sim 1/\rho^2$ for the Efimov effect. The hyperradius ρ is proportional to the square root of the sum of all interparticle distances weighted with their corresponding reduced masses, $\rho = \sqrt{\sum \mu_{ij} r_{ij}^2}$ with (μ_{ij} in units of the nucleon mass). When we deal with a Borromean halo, the neutron-neutron interaction with scattering length ~ 16 fm is decisive for this effect (also called "continuum pairing"). Additionally, in the ^{11}Li case, the presence of an intruder virtual *s* level (antibound) in ^{10}Li gives a large (but still not fully known) scattering length, which contributes essentially to the abnormally large matter r.m.s. radius.

For three-body systems, a residual three-body centrifugal barrier $\frac{15}{4}\hbar^2/(2m\rho^2)$ is present, even in case of the smallest hypermoment $K = 0$ with zero intrinsic binary angular momenta (except for the Efimov regime). This gives, in contrast to a binary system, the possibility for the existence of narrow low-lying "*s*"-wave resonances with pair angular momenta equal to zero.

An abnormally large correlation distance could also be realized by a long-living binary resonance propagating to a large distance, as well as from a binary virtual (antibound) state. In this case, no concentration of the three-body wave function inside the region of interaction of all constituents will take place, but there will be a long-range spreading of correlations.

The Appendix summarizes relevant formalism using the Jacobi relative momentum coordinates $\mathbf{k}_x$ and $\mathbf{k}_y$, used to describe the scattering states of three-body systems, and gives

also the plane wave and distorted continuum wave functions, including final state interactions (FSI), of three-body systems consisting of a spinless core and two nucleons. We henceforth use the notation defined in the Appendix for three-body wave functions and S-matrix elements.

B. Defining energy correlations

In general, all possible correlations are contained in the scattering amplitudes. In this paper we focus on the simplest (but very important) characteristics, the angular-integrated energy correlations. From a theoretical point of view, we should clearly use Jacobi coordinates to describe internal excitations of the system and corresponding energies of relative motion between two particles (ϵ_{xi}) and for their c.m. relative to the third one (ϵ_{yi}). Among three Jacobian systems $\{i\}$ only two are essentially different because of the identity of the two halo neutrons. In the **T** system we use the neutron-neutron relative motion energy $E_{nn} = \epsilon_{xi}$ and the energy between the core (c) and the c.m. of the two neutrons, $E_{(nn)-c} = \epsilon_{yi}$. In the **Y** system ("shell model") we use the neutron-core relative motion energy $E_{cn} = \epsilon_{xj}$ and the energy between their c.m. and the second neutron, $E_{(cn)-n} = \epsilon_{yj}$.

Angular-integrated correlation functions characterising the low-energy continuum can be obtained from the partially integrated cross sections of Eq. (A16) for $3 \to 3$ scattering (which reflects intrinsic properties of the continuum), if we integrate these over the directions of the incident particles, the distribution of the total energy between them (Ω_5^κ), and also over the directions of scattered particles ($d\hat{\mathbf{k}}_x^{\mathbf{f}} d\hat{\mathbf{k}}_y^{\mathbf{f}}$). After integration and summation over the projection M of the total angular momentum J, the differential cross section describing the distribution of total energy $E = \epsilon_{x_i} + \epsilon_{y_i}$ by subsystems x_i, y_i will be an incoherent sum over the quantum numbers of the incident particles as well as the angular momenta of the scattered ones:

$$\frac{1}{\sin^2 \alpha_f \cos^2 \alpha_f} \frac{d\sigma(3)}{d\alpha_f}$$
$$= \frac{2}{\pi \kappa^5} \frac{1}{(2s_1 + 1)(2s_2 + 1)} \sum_{JK\gamma\gamma'} (2J + 1)$$
$$\times \left| \sum_{K'} \left(\delta_{K\gamma;K'\gamma'} - S_{K\gamma;K'\gamma'}^J \right) \psi_{K'}^{l'_x l'_y}(\alpha_f) \right|^2. \quad (1)$$

Since the S matrix in the $3 \to 3$ scattering amplitude of Eq. (A14) has instructive analytic properties, and because we want to study energy correlations coming from intrinsic properties of the three-body continuum, we will omit the strong energy dependence $\sim \kappa^{-5}$, which can generate artificial bumps in cross sections (see Sec. III E). By taking into account that $\sin^2 \alpha_f = \epsilon_x / E$, a correlation function can be defined as a function of $\epsilon_{x_i}, \epsilon_{y_i}$ at a fixed $E = \epsilon_{x_i} + \epsilon_{y_i}$:

$$B_{\text{intr}}^J(\epsilon_x, \epsilon_y) = \sum_{K\gamma\gamma'} \left| \sum_{K'} \left(\delta_{K\gamma;K'\gamma'} - S_{K\gamma;K'\gamma'}^J(E) \right) \psi_{K'}^{l'_x l'_y}(\alpha_f) \right|^2. \quad (2)$$

For small ($\epsilon_{xi}, \epsilon_{yi}$), the behavior of the correlation function is defined by the lowest partial angular momenta l_x, l_y of the state J^π via multipliers $(\epsilon_{xi})^{l_x}(\epsilon_{yi})^{l_y}$ arising from the product of the hyperangular parts of hyperspherical functions $\psi_K^{l_x l_y}(\alpha_i)\psi_{K'}^{l_x l_y}(\alpha_i)$—see Eq. (A4).

To compare with the energy correlations extracted from nuclear reactions we will also use a correlation function corrected for the three-body phase volume

$$B_{\text{reac}}^J(\epsilon_x, \epsilon_y) = \sqrt{\epsilon_x \epsilon_y} \, B_{\text{intr}}^J(\epsilon_x, \epsilon_y). \quad (3)$$

This phase space factor $\sqrt{\epsilon_x \epsilon_y}$ will affect only the behavior of correlations at small values of ϵ_x, ϵ_y.

Borromean nuclei, represented as core $+ n + n$, should in the "shell-model" **Y** coordinate system have a correlation function that is almost symmetrical about the hyperangle $\alpha_Y \sim 45^\circ$ ($\epsilon_x = \epsilon_y$) because of the antisymmetry between the valence nucleons, but with a correction depending on finite masses, which is a recoil effect that vanishes in the limit of an infinitely heavy core to give then a symmetrical correlation function.

C. Energy correlations from resonances in $3 \to 3$ scattering

The intrinsic properties of the halo continuum are contained in the scattering amplitudes that characterize the asymptotics of the wave functions at large distances.

The scattering amplitude may in general have several kinds of analytical singularities corresponding to long-living states, but we will concentrate on two of them, the most physically transparent [32] (where for simplicity of notation we omit the spin indices):

(i) A "true" three-body resonance for given J^π is one, for which the $3 \to 3$ scattering amplitude f^J of Eq. (A13) has the analytical property (a simple pole)

$$f^J\left(E, \Omega_5^\rho, \Omega_5^\kappa\right) \sim \kappa^{-5/2} \frac{A^J\left(\Omega_5^\rho, \Omega_5^\kappa\right)}{E - (E_0 - i\Gamma_0/2)}, \quad (4)$$

where E is the total energy calculated from three-body threshold, and E_0 and Γ_0 are, respectively, the position and width of the resonance pole.

For wide resonances we can expect the same resonant structure to appear in part of the S-matrix elements distorted by a background.

The resonant structure of the wave function in coordinate space is manifested as a pronounced enhancement according to a Breit-Wigner form with the same E_0 and Γ_0 in the interior region, as discussed in (I).

(ii) In absence of a "true" three-body resonance, remnants of two-body resonances in the binary subsystems may produce amplification with a simpler analytical structure. A rather general expression, in the case of a long-living resonant state in one binary subsystem that interacts weakly with the third particle, is

$$f^J\left(E, \Omega_5^\rho, \Omega_5^\kappa\right) \sim \kappa^{-5/2} A_2^J\left(\Omega_5^\rho, \Omega_5^\kappa\right) \frac{c_\beta(E)}{\epsilon - (\tilde{\epsilon} - i\tilde{\Gamma}/2)}. \quad (5)$$

Here β labels the quantum numbers of the binary resonance, ϵ is the part of the total energy E shared by the resonant binary subsystem, and $\tilde{\epsilon} - i\tilde{\Gamma}/2 = \epsilon_0 + \Delta\epsilon - i(\tilde{\Gamma}_0/2 + \Delta\Gamma/2)$ with ϵ_0 and Γ_0 being the position and width, respectively, of the binary resonance without the presence of the third particle. The term $\Delta\epsilon - i\Delta\Gamma/2$ is the shift and additional width caused by the coupling with the third particle. The amplitude $c_\beta(E)$ is some smooth function of the total energy E. We can also use this expression for a binary virtual (antibound) state, keeping in mind that it can be approximately represented as a near-threshold resonance.

To gain a qualitative understanding, we can apply these analytic properties to the $3 \rightarrow 3$ scattering amplitudes to obtain the prototypical behavior for cases 1 and 2. We first expand the energy dependent part of scattering amplitude $A(E, \Omega_5^\rho, \Omega_5^\kappa)$ in terms of hyperspherical harmonics (A2) with coefficients $A_{K\gamma;K'\gamma'}^{J(3)}$ derived from a pole of the S-matrix

$$\frac{A_{K\gamma;K'\gamma'}^{J(3)}}{E - (E_0 - i\Gamma_0/2)} = \delta_{K\gamma;K'\gamma'} - S_{K\gamma;K'\gamma'}^{J}(E), \qquad (6)$$

where $K\gamma$ labels the Ω_5^κ asymptotic component of the ingoing waves, and $K'\gamma'$ labels the rescattered wave at Ω_5^ρ. For a narrow true three-body resonance the correlation function (2) simplifies to the transparent form

$$B_{\text{intr}}^{J}(\epsilon_x, \epsilon_y) \sim \frac{1}{(E - E_0)^2 + \Gamma_0^2/4} \sum_{K'\gamma'} \sum_{K\gamma, K''} A_{K\gamma;K'\gamma'}^{J(3)} A_{K\gamma;K''\gamma''}^{*J(3)}$$

$$\times \chi_{K'}^{l_x' l_y'}(\epsilon_y, \epsilon_x) \chi_{K''}^{l_x' l_y'}(\epsilon_y, \epsilon_x). \qquad (7)$$

Since $E = \epsilon_{xi} + \epsilon_{yi}$ is invariant (i.e., the same in any Jacobi system i), it is clear that a correlation plot of $B_{\text{intr}}^{J}(\epsilon_x, \epsilon_y)$ should have a maximum along the straight line $E_0 = \epsilon_{xi} + \epsilon_{yi}$ for narrow resonances and sections in a contour plot of elliptical type with width $\sim \Gamma_0$. The general behavior is defined by the partial structure of the state contained in the *lowest K* components of the hyperangular part of the wave function $\chi_K^{l_x l_y}(\epsilon_y, \epsilon_x) \sim \sqrt{\epsilon_{xi}^{l_x} \epsilon_{yi}^{l_y}} P_{(K-l_x-l_y)/2}^{l_x+1/2,l_y+1/2}(\frac{\epsilon_y - \epsilon_x}{E})$, where P is a Jacobi polynomial [see (A4)]. Small values of ϵ_y, ϵ_x are indicators of partial content of the state in the correlation function since it is defined by kinematical factors $\sim \epsilon_x^{l_x}$ and $\sim \epsilon_y^{l_y}$ from the lowest binary angular momenta. An example of a true three-body resonance is the 2_1^+ state in ^{6}He, discussed in Sec. III A.

For the case of the correlation function of Eq. (3) with phase space factors included, the plot will be modified by the factor $\sqrt{\epsilon_{xi} \epsilon_{yi}}$ which shifts the maxima line from resonance position by $\delta E \cong \Gamma_0^2/4E_0$ and changes the maxima behavior along the ridge, suppressing the correlation function at small values of $\epsilon_{xi}, \epsilon_{yi}$.

For a two-body resonance in one of the binary subsystems, we may neglect all partial waves except the one set $\{l_x, l_y\}$ containing the resonance [32] and use the Jacobi system with the x coordinate corresponding to the resonant pair. Integrating over angles [using the "reaction" expression (3), which is

a prototype for transition correlations] yields a correlation function with the following functional form:

$$B_{\text{reac}}^{J}(\epsilon_x, \epsilon_y) \sim \frac{F_3(E)(\epsilon_{xi}/E)^{l_x} \sqrt{\epsilon_{xi} \epsilon_{yi}}}{(\epsilon_{xi} - \tilde{\epsilon}_i)^2 + \Gamma_i^2/4}, \qquad (8)$$

where the amplitude $F_3(E)$ is a smooth function of E. The corresponding correlation plot has in this case characteristic maxima along the straight line $\epsilon_{xi} = \tilde{\epsilon}_i$ perpendicular to the ϵ_{xi} axis, and with behavior defined by phase space and the partial angular momentum $l_x \neq 0$ giving multipliers $(\epsilon_{xi})^{l_x}$. For $l_x \neq 0$ or $l_y \neq 0$ the maxima line $\epsilon_{xi} = \tilde{\epsilon}_i$ will be shifted to larger ϵ_{xi} energies. We note that to reproduce a binary long-living resonance we need a large number of hyperspherical harmonics.

To transform from an initial (say **T**) to another (**Y**) Jacobi system, we should use the full transform relations [see Eq. (A10)] for momenta $\mathbf{k}_x, \mathbf{k}_y$ (i.e., not an expression integrated over angles). In the vicinity of the resonance energy $\tilde{\epsilon}_i$, however, the only fast-varying quantity is the resonant denominator. Therefore we will simply replace ϵ_{xi} in the denominator of Eq. (8) by $\epsilon_{xj} \sin^2 \phi_{ij} + \epsilon_{yj} \cos^2 \phi_{ij} + (\hbar^2/m)\mathbf{k}_{xj} \cdot \mathbf{k}_{yj} \sin \phi_{ij} \cos \phi_{ij}$ and then integrate over angles in the rotated system. In the numerator of Eq. (8) only partial angular momenta l_x and l_y will be changed, while conserving the parity and total orbital momentum L, so the total energy E and phase space will be the same. Then we should integrate the rotated cross section over the new angles. For simplicity we average the scalar product $(\mathbf{k}_{xj} \cdot \mathbf{k}_{yj})$ in the denominator over angles, which gives approximately zero. This results in a maximum curve in Eq. (8) along a straight line $\tilde{\epsilon}_i = \epsilon_{xj} \sin^2 \phi_{ij} + \epsilon_{yj} \cos^2 \phi_{ij}$, looking similar to that from a three-body resonance, but with inclination angle defined by the ratio of mass numbers, $\tan^2 \phi_{ij} = A_k(A_i + A_j + A_k)/A_i A_j$, and with contour plot of elliptical type with "width" $\sim \Gamma_i$.

The prototype behavior for a system like ^{6}He or ^{11}Li with a resonance (and an approximate virtual state) in the two-body subsystems is illustrated in Fig. 1 for the three-body dipole-type excitation $J^\pi = 1^-$. We choose the dipole three-body continuum because it corresponds to final states that can be excited by Coulomb E1 excitation from the 0^+ g.s. of Borromean systems. The structure $l_x = 0, l_y = 1$ in the final continuum state will be energetically preferable in the **T** partition owing to the $n-n$ virtual state and in the **Y** partition it becomes an almost symmetric mixture of $l_x = 0, l_y = 1$ and $l_x = 1, l_y = 0$.

The lower part of Fig. 1 shows the energy correlation induced by a core-n resonance in the $l = 1$ partial wave, typical for p-shell nuclei. The maximum line for constant ϵ_{xj} transforms to the line $\tilde{\epsilon}_i = \epsilon_{xj} \sin^2 \phi_{ij} + \epsilon_{yj} \cos^2 \phi_{ij}$ in the **T** system, resembling a three-body resonance, but the inclination angle is not $\pi/4$ as for a three-body resonance.

In the upper part of Fig. 1 the position of the binary resonance is chosen near the threshold, so that it simulates the energy dependence of the $l_x = 0$ virtual state in the nn system, with almost zero interaction between the nn pair and the third particle. The visible maxima line for constant ϵ_{xj} in the **T** Jacobi system transforms in the **Y** Jacobi system to an oval
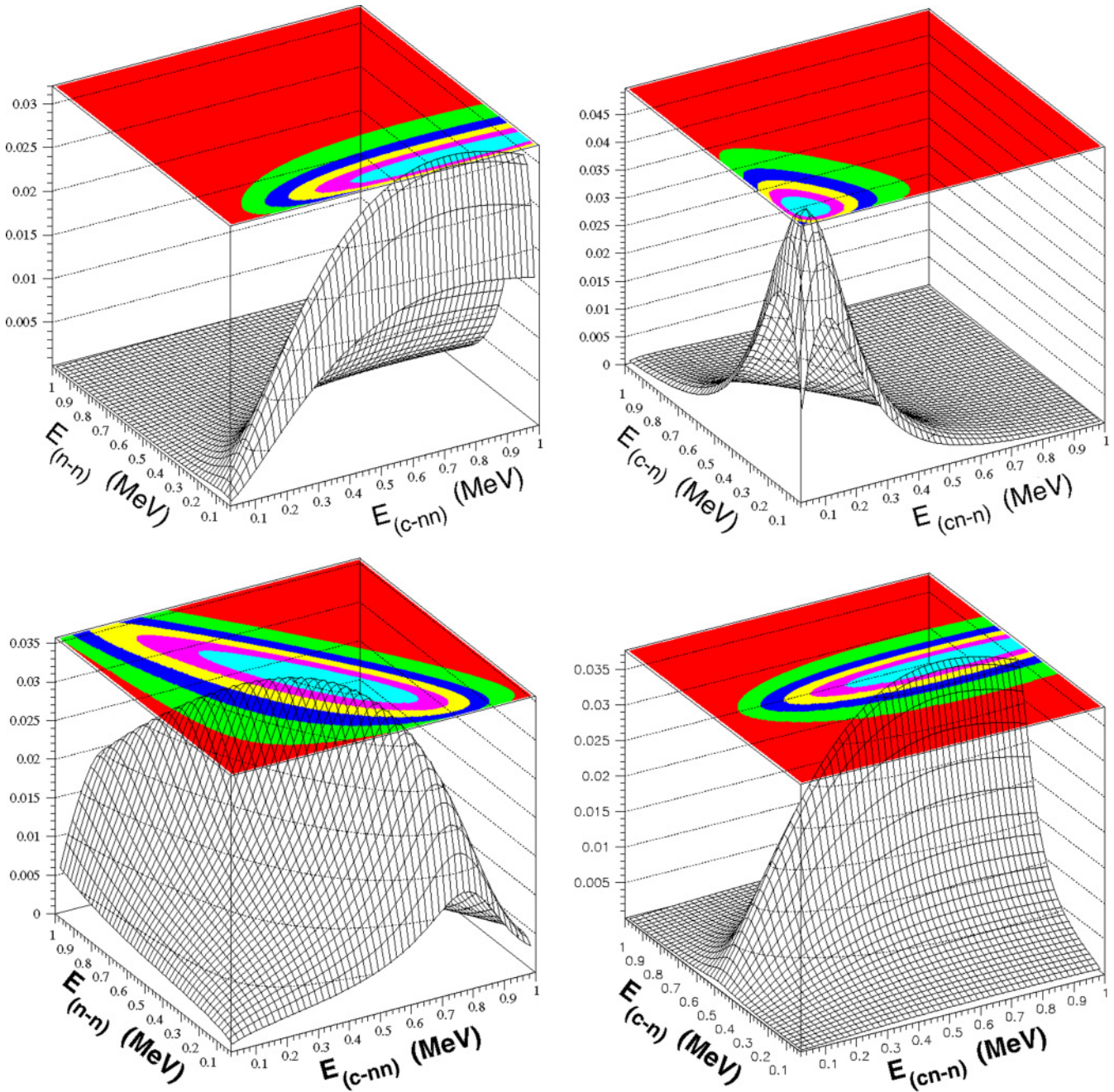
FIG. 1. (Color online) Prototype dipole energy correlations for a two-body resonance and a virtual state in a three-body dipole continuum, modeled from the analytical properties of the scattering amplitude. Upper row: induced by a virtual (antibound) state in the *nn* subsystem. Lower row: induced by a low-lying core-*n* two-body resonance. Left column: in cluster **T** basis; right column: in "shell-model" **Y** basis.

in the vicinity of the origin. This asymmetric transformation can serve as a discriminating tool in doubtful cases, when in the total cross section there is a bump of unknown nature.

It should be mentioned here that in reality the resonance component will always contain some nonresonant background.

Using the example of ^{6}He we shall demonstrate the most important cases of three-body energy correlations:

(i) energy correlations for narrow resonances;

(ii) energy correlations for wide resonances; and

(iii) energy correlations for three-body virtual-like excitations, which are characterized by a fast increase of the lowest eigenphase at small energies (with subsequent decrease) but not crossing $\pi/2$, in contrast to the case of a resonance [2].

In more complicated cases, when we have only a resonant-like enhancement in the main partial cross-sections, we need additional observables using the correlation responses.
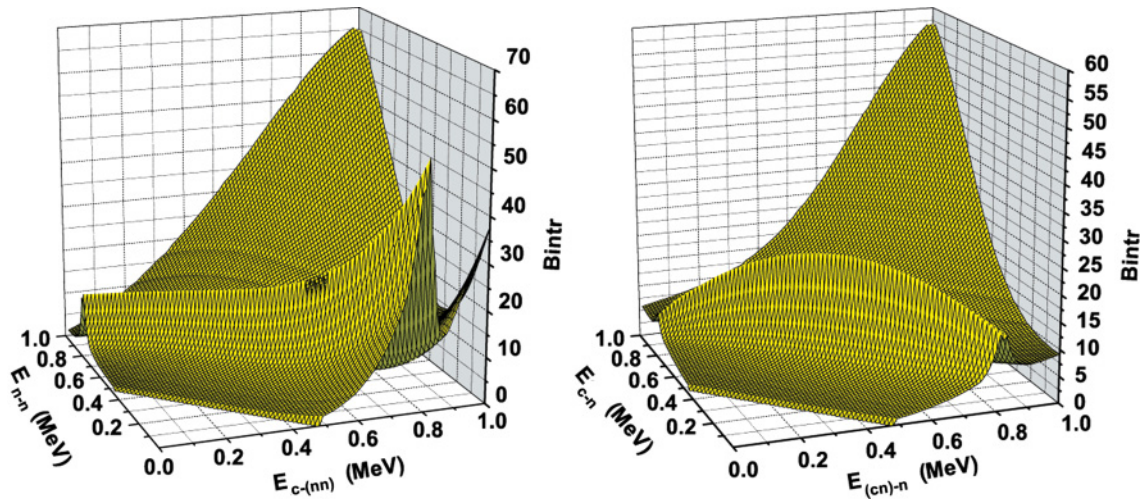
FIG. 2. (Color online) Intrinsic energy correlation plot for the 2_1^+ resonance of ^{6}He: in **T** basis (left) and in **Y** basis (right).

III. ENERGY CORRELATIONS IN ^{6}He

A. The 2_1^+ resonance

The clearest case of a three-body resonance is the well-known 2_1^+ resonance at 0.8 MeV above the three-body threshold. The correlation plots in Figs. 2 and 3 show this classic example of a three-body resonance, where in both coordinate systems the maximum contours follow the rule $E_0 = \epsilon_{xi} + \epsilon_{yi} = 0.84$ MeV, derived from the analytic structure of the scattering amplitude. The $K = 2$ components give almost the full width of this state. The partial structure is discussed in detail in [2].

From the asymmetric shape in $n-n$ and $\alpha-nn$ coordinates (**T** basis in Fig. 2 we can see that the preferable mode of the resonance decay is an s-wave one with small relative

energy between neutrons, since the angular momentum $l_x = 0$ gives nonzero value of the correlation function [Eq. (2)] $B_{\rm int} \sim (\epsilon_{xi})^{l_x} \neq 0$ at small $\epsilon_{xi} = E_{n-n}$. At the same time almost all the resonance energy will be contained in the $\alpha - nn$ relative d-wave motion ($l_y = 2$). At small $\epsilon_{yi} = E_{c-(nn)}$, s-wave motion with $l_y = 0$ will also be enhanced owing the factor $(\epsilon_{yi})^{l_y} = 1$ in the correlation function. These features demonstrate the dominance of the configurations $l_x = 0, l_y = 2$ and $l_x = 2, l_y = 0$ in the vicinity of resonance energy, with the former being twice as pronounced.

The correlation plot in the **Y** basis is almost symmetric about the angle $\pi/4$, in accordance with the antisymmetrization of the valence neutrons. The large admixture of $l_x = 0$ ($l_y = 0$) components at small E_{c-n} ($E_{(cn)-n}$) is a manifestation of $s-d$ shell admixture and recoil effects. The intermediate
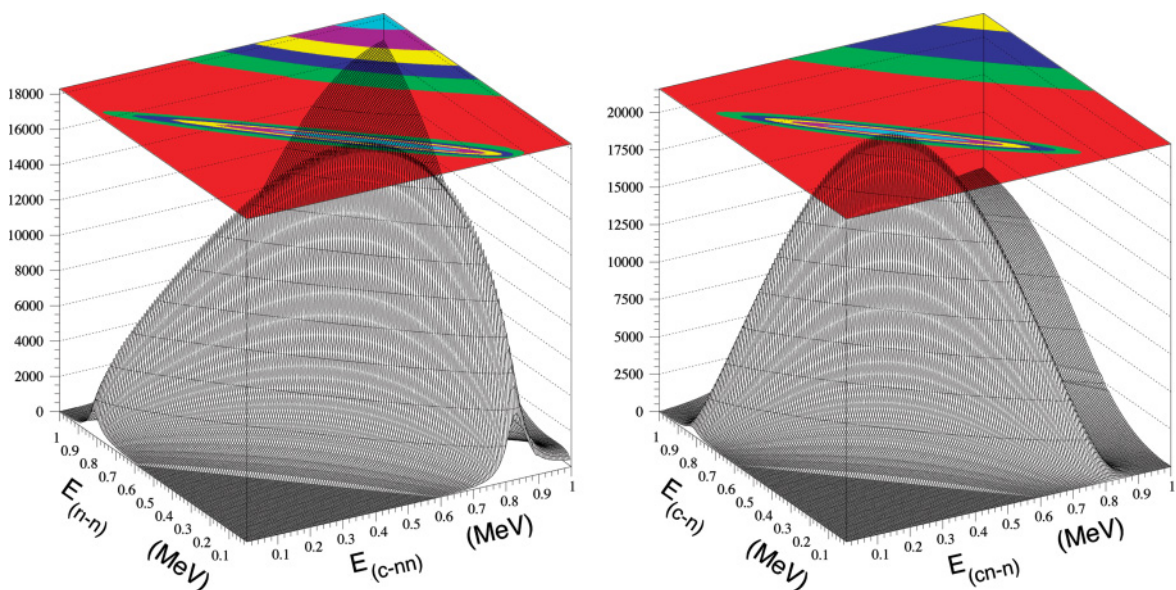

FIG. 3. (Color online) Energy correlation plot for 2^+ resonance with three-body phase space included in cluster **T** basis (left), and in "shell-model" **Y** basis (right).
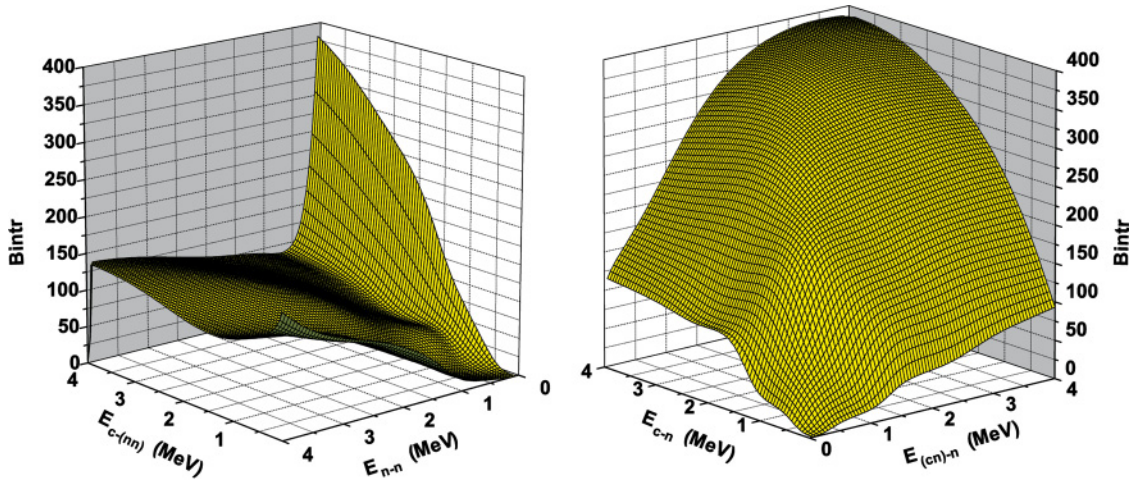
FIG. 4. (Color online) Intrinsic energy correlation plot for 0^+ states in cluster **T** basis (left) and in "shell-model" **Y** basis (right). Note the reversed axes of the left plot.

energy shape of the correlation function is mostly defined by $l_x = 1, l_y = 1$ in accordance with the dominant $(p_{3/2})^2$ component in the resonance structure of 2^+ state in the **Y** basis.

The situation changes when the phase space is included, as shown in Fig. 3. The influence of phase space on the visible resonance position is negligible, but in the **T** basis the amplification of the s-wave $n-n$ correlation at small E_{n-n} is overridden by the phase space factor, as is also the s-wave behavior at small $E_{c-(nn)}$. Nevertheless, the asymmetric shape of the correlation plot along the ridge gives an indication of a preferable decay with smaller relative $n-n$ energy and larger $c - nn$ energy. In the **Y** basis, the phase space factor suppresses the s-wave behavior at small E_{c-n} and $E_{(cn)-n}$ but does not significantly change the profile of the correlation function.

At higher energy both plots show the appearance of the second 2^+ resonance.

B. Monopole 0^+ continuum

The monopole 0^+ intrinsic continuum correlations (Fig. 4) show no presence of three-body resonant behavior, but they do reflect a strong influence of FSI. Figure 4 demonstrates in the cluster **T** basis an extremely narrow s-wave peak along the small E_{n-n} energy. This peak resembles the schematic case of a virtual binary state (Fig. 1) and is even more evident when the phase space is included (Fig. 5). The s-wave behavior also dominates at small $E_{c-(nn)}$ energy.

In the **Y** basis an oval-shaped peak was expected in accordance with the qualitative picture of Fig. 1, but only a monotonically growing background can be seen in Fig. 5. To explain this feature, and also the cases of wide 2_2^+ and 1^+ resonances, we can draw an analogy with two-body scattering. There, only the impact parameters that are less then the size of interaction region contribute to the scattering cross section. In the three-body case the hyperradius ρ, hypermoment K, and hypermomentum $\kappa(=\sqrt{2m(\epsilon_{xi} + \epsilon_{yi})/\hbar^2})$ play the same respective roles as r, L, and k of the two-body case. For example, if we take a radius ρ_0 of the three-body interaction region of about 5 fm, and a continuum energy of about 2 MeV,

then $K \sim \kappa\rho_0 \sim 1.5$. Because of channel couplings, however, higher K (corresponding to larger values of the impact parameter) can add some contribution to the background.

We can make a filter for those partial waves for which the impact parameter matches the interaction radius in the energy range of interest. The result for the leading $K = 2$ terms (in- and outgoing) is presented in Fig. 6. In the **T** basis there are two pronounced wings corresponding to correlated motion of two neutrons with small energy E_{n-n} of relative motion and small $E_{c-(nn)}$ energy between the two neutrons and the core. Interference with the structureless $K = 0$ component will reduce the $c-(nn)$ peak and increase the $n-n$ peak. In the **Y** basis there is not quite so pronounced a peak at $E_{c-n} \sim E_{(cn)-n} \sim 1.2$ MeV, in accordance with a qualitative analysis of the binary resonance and virtual state, and this is almost smeared out after adding components with higher K. Including the higher K values adds $\sim 50\%$ to the background at energies $E_{n-n}, E_{c-(nn)} > 2$ MeV, while conserving the peak structure.

Nevertheless, the long-range spatial correlations up to ~ 20 fm in the three-body monopole continuum, as discussed at Ref. (I), manifest themselves as pronounced $n-n$ energy correlations with small E_{n-n}, and as $c-(nn)$ energy correlations at small $E_{c-(nn)}$ (partially) smeared by the background, both with pair angular momenta $l_x, l_y = 0$. Physically this corresponds to a significant part of the decay probability proceeding via the neutron-neutron s-wave virtual state.

In contrast, the kinematics of the decay in the **Y** basis does not show a definite decay via the $p_{3/2}$ resonance in ^{5}He located at 0.8 MeV. This can be understood qualitatively as changing the predominant $p_{3/2}^2$ structure of the g.s. to $p_{1/2}^2$ plus $s_{1/2}^2$ in the low-energy continuum.

As expected from qualitative considerations, the mirror 0_2^+ state (orthogonal in angular-spin content to the ground state) has a predominant $S = 1$ component, which should have a symmetric shape in the correlation plot because of its angular momentum structure. It should have $l_x = l_y = 1, L = 1$ in both systems, in contrast to a monopole breathing mode where $S = 0, l_x = l_y = 0, L = 0$ in $\alpha-nn$ (i.e., the $n-n$ **T** system) and $l_x = l_y = 1, L = 0$ in $n-\alpha$ [i.e., the $(n\alpha) - n$ **Y** system].
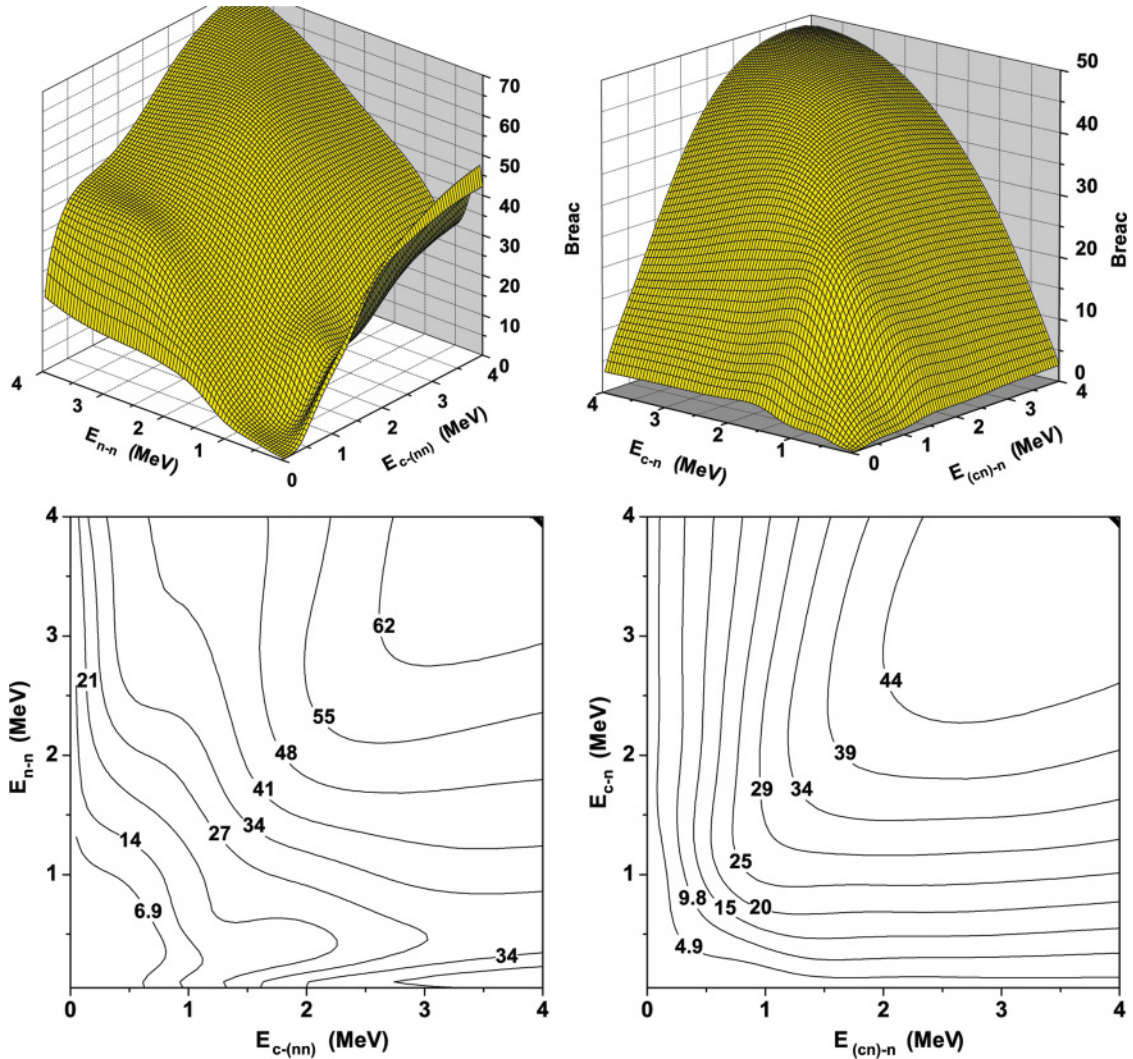
FIG. 5. (Color online) Energy correlation plot for 0^+ states with three-body phase space included in cluster **T** basis (left) and in "shell-model" **Y** basis (right). Lower panels give contour plots of upper panels.
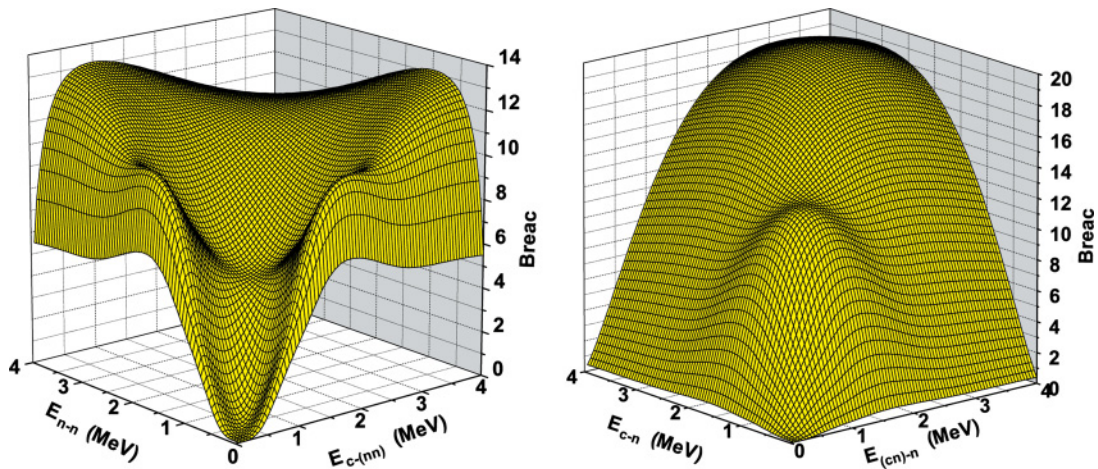

FIG. 6. (Color online) Energy correlation plot for 0^+ state for only $K = 2$ with three-body phase space included: in cluster **T** basis (left), in and "shell-model" **Y** basis (right).
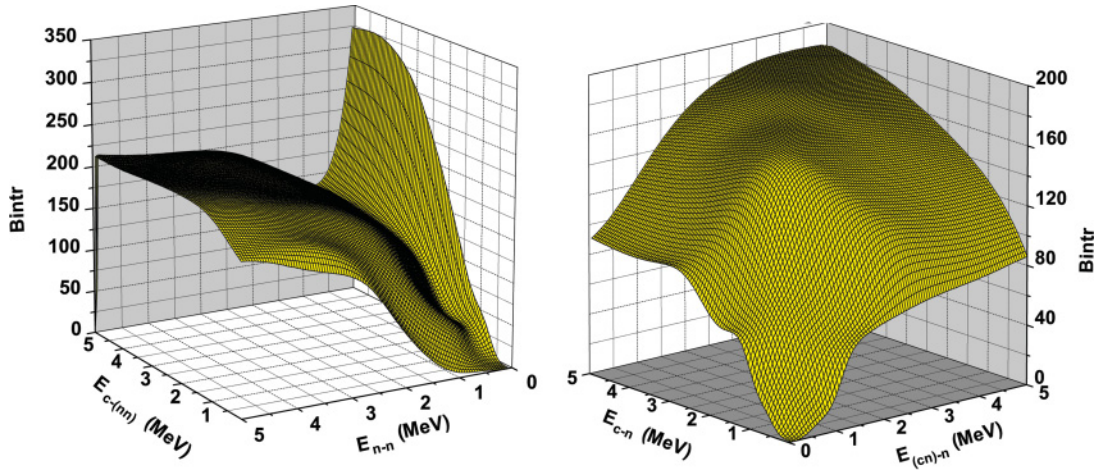
FIG. 7. (Color online) Intrinsic energy correlation plot for the 1^- continuum in cluster **T** basis (left) and in "shell-model" **Y** basis (right).

From S-matrix analyses and correlation properties, we find that it does not exist as a sufficiently narrow resonance, because of spreading into the continuum.

C. Dipole 1^- continuum

Analysis of eigenphases for the dipole continuum in Ref. [2] has shown the three-body virtual-like character of this excitation. The dipole correlations (Fig. 7) are very similar to those of the monopole. At small pair energies of relative motion the s wave prevails in both **T** and **Y** bases. Also, as in the 0^+ case, in the **T** basis there is a very narrow ridge along small energies E_{n-n} of $n-n$ relative motion. This ridge also comes when all states with $K = 1$–11 are included, which is a signal of the binary decay mode via the $n-n$ virtual state. Spatial correlations in the three-body continuum are again of long range [8]. The $\alpha-nn$ energy distribution has s-wave behavior at small $E_{c-(nn)}$ from admixed $l_{\alpha-nn} = 0$.

In the **Y** basis, an oval-shaped peak was expected in accordance with the qualitative picture of Fig. 1. As in the

monopole case, only a monotonically growing background can be seen in Fig. 7. The kinematics of the decay in the **Y** basis does not show a definite decay via the $p_{3/2}$ resonance in the ^{5}He. This can be understood qualitatively as a competition between $p_{3/2}$ and $s_{1/2}$ waves in the ^{5}He subsystem, owing to the predominant $p_{3/2}s_{1/2}$ structure in the **Y** basis of the ^{6}He dipole continuum.

We applied a filter for partial waves with $K = 1, 3$, corresponding to a matching of the impact parameter with surface values of the interaction radius. In the **T** basis there is a structureless picture (not shown) with small amplification of s-wave motion with small E_{n-n}. In the **Y** basis, as in the 0^+ case, there is a not so pronounced peak at $E_{c-n} \sim E_{(cn)-n} \sim 2$ MeV, which is almost smeared out after adding components with higher hypermomenta K.

A structure very similar to that of 0^+ appears when the phase space factor is included in the energy correlations. In Fig. 8 there is a clearly seen $n-n$ ridge, corresponding to decay via the s-wave virtual state, but it is not so pronounced as in 0^+ correlations.
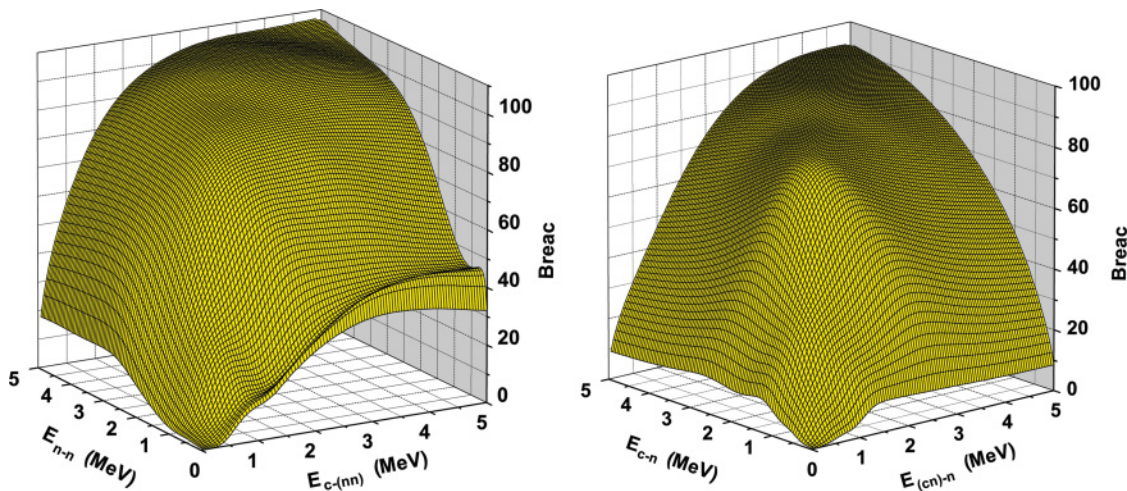

FIG. 8. (Color online) Energy correlation plot for the 1^- continuum with three-body phase space included in cluster **T** basis (left) and in "shell-model" **Y** basis (right).
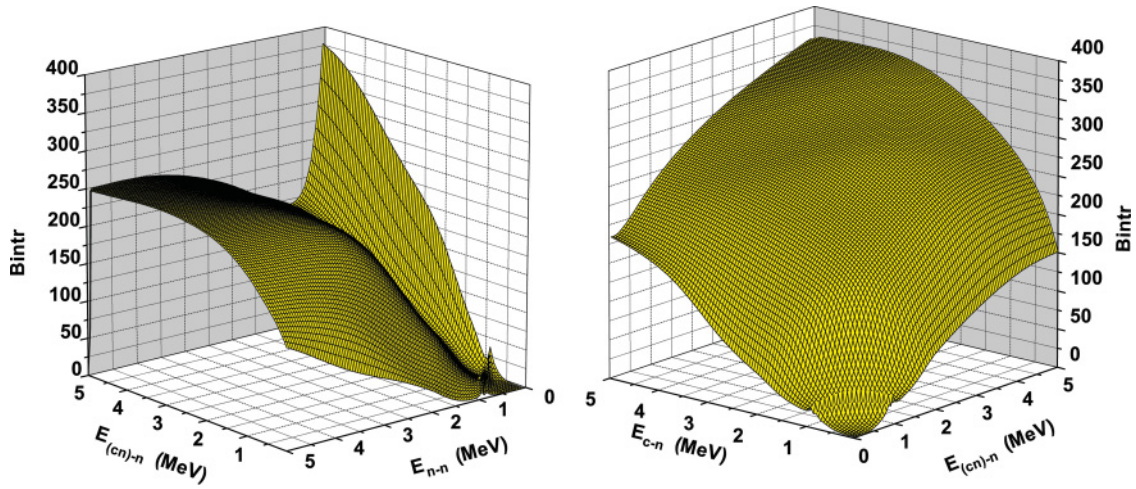
FIG. 9. (Color online) Intrinsic energy correlation plot for 2_2^+ state in cluster **T** basis (left) and in "shell-model" **Y** basis (right). Note the 2_1^+ small peaks along the ridge $E_{c-(nn)} + E_{n-n} = E_{(cn)-n} + E_{c-n} = 0.8$ MeV.
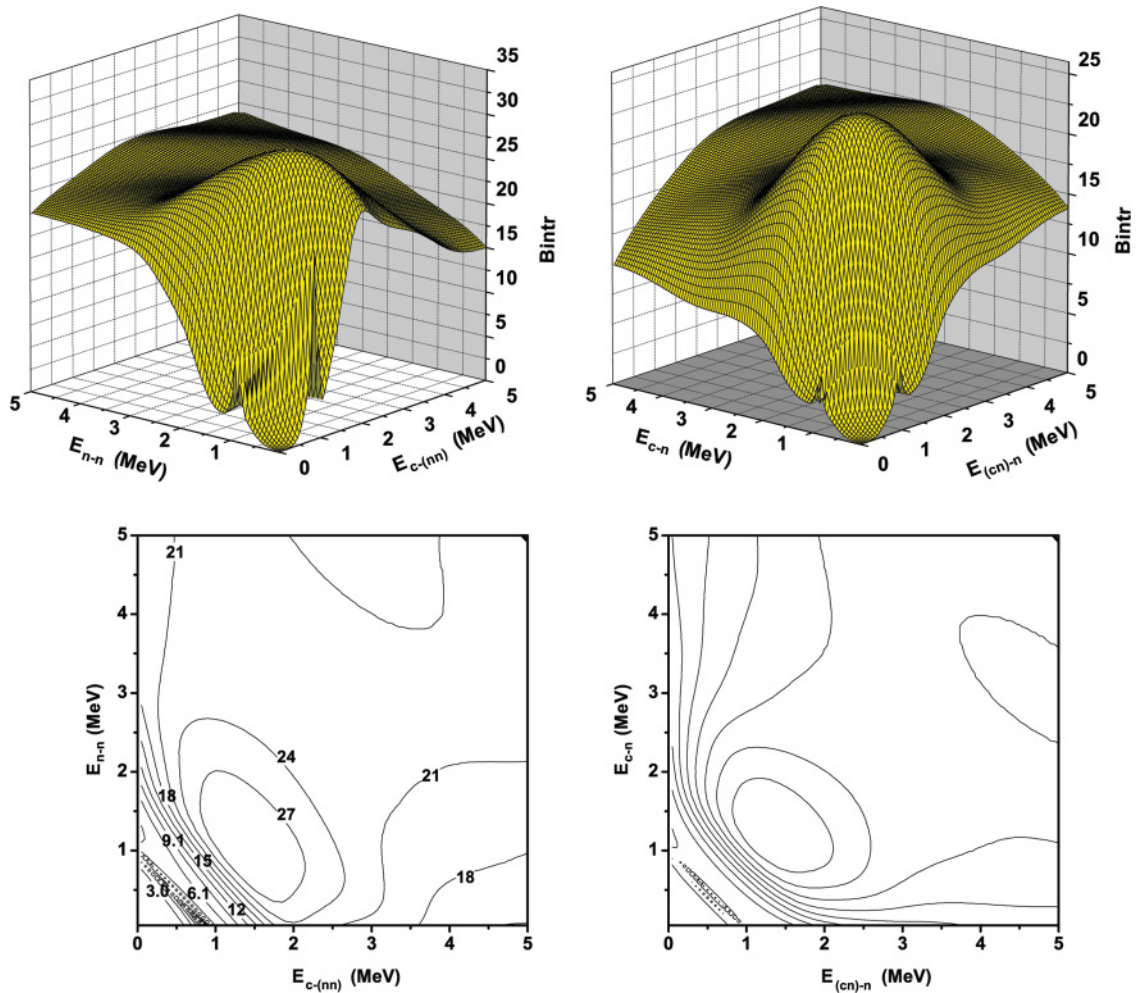

FIG. 10. (Color online) Intrinsic energy correlation plot for 2_2^+ resonance for only $K = 2$ in cluster **T** basis (left) and in "shell-model" **Y** basis (right). Lower panels give contour plots of upper panels.

FIG. 11. (Color online) Intrinsic energy correlation plot for the 1^+ state in cluster **T** basis (left) and in "shell-model" **Y** basis (right).

FIG. 12. (Color online) Intrinsic energy correlation plot for 1^+ resonance for only $K = 2$ in cluster **T** basis (left) and in "shell-model" **Y** basis (right). Lower panels give contour plots of upper panels.
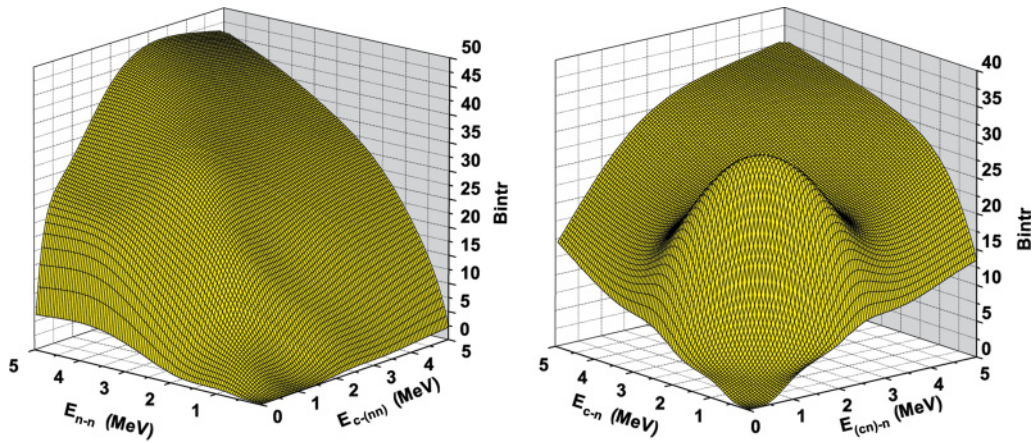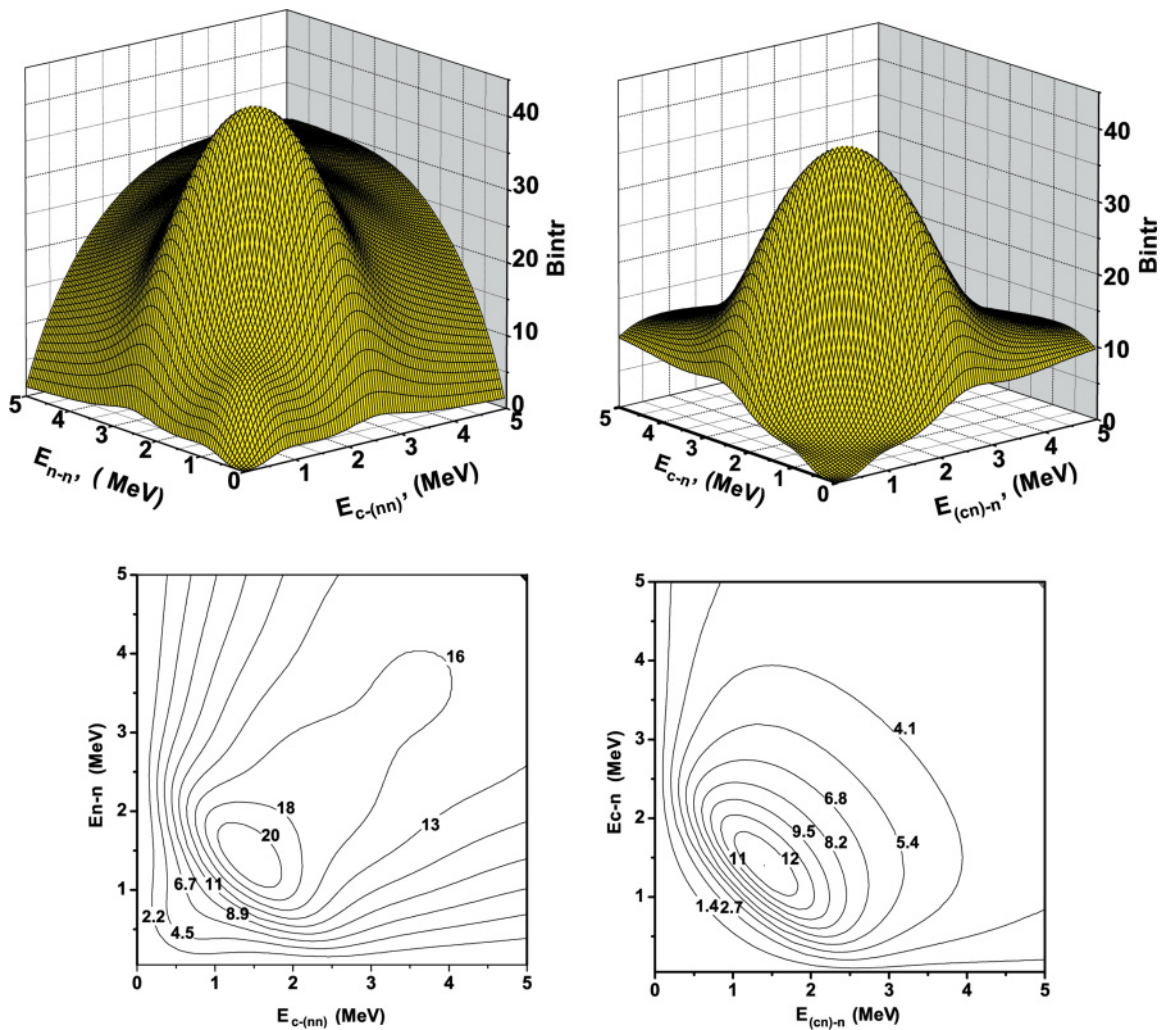
D. Summary

The analysis performed here has confirmed that the well-known 2_1^+ state is a real three-body resonance. Three-body correlations for all configurations have demonstrated that, in spite of presence of a soft dipole resonance-like peak in both nuclear and electromagnetic response functions at ~1.5 MeV, there is a lack of noticeable resonant behavior in the interior region (as is also true for the monopole case). The physical reasons are quite different. In the monopole case, it is the spreading into the continuum caused by dominating s motion between the two halo neutrons, and because of less expressed s motion between the correlated nn pair and the core. In the dipole case, there is almost complete cancellation in the three-body matrix elements in ρ between the s-wave repulsion and p-wave attraction between the halo neutrons and the α particle. Thus the s-wave nn attraction alone dominates the dynamics, and the structure of this mode is quite similar to 0^+, being defined by p-wave motion between the core and a correlated nn-pair with relative angular momentum $l_{nn} = 0$.

E. Second 2_2^+ resonance

In addition to the sharp 2_1^+ resonance at 0.8 MeV above threshold, the calculations gave a wide second 2_2^+ resonance. It is most interesting that the resonant behavior appears largely in one partial **T** component $K = 2, L = 2, S = 0, l_x = 2, l_y = 0$, at a continuum energy of 2.3 MeV and a width $\Gamma \sim 1.4$ MeV. The eigenphase of the lower 2_1^+ resonance crosses $\pi/2$ at an energy of 2 MeV, which is within the width of the 2_2^+ resonance [33].

Intrinsic energy correlations are presented in Fig. 9. In both plots one can also see the very narrow 2_1^+ resonance at 0.8 MeV, now with a somewhat distorted peak caused by the larger (0.1 MeV) energy step in this plot. At higher energies this plot is very similar to plots of energy correlations in the 0^+ and 1^- continua.

After filtering out the background to leave only the $K = 2$ partial wave, the resonant structure became evident. As in the 2_1^+ case, the plot in Fig. 10 has an asymmetric shape in the **T** basis with dominating $K = 2, L = 1, S = 1, l_x = l_y = 1$ component strongly influenced by the "binary" $(n-n)$ decay channel with $K = 2, L = 2, S = 0, l_x = 0, l_y = 2$, analogous to 0^+ and 1^- cases. In the **Y** basis there is a strong component with the same $K = 2, L = 1, S = 1, l_x = l_y = 1$ configuration, giving a symmetric shape, but for 2^{+_1} states other significant components ($L = 2, S = 0, l_x = 0, l_y = 2$ and $L = 2, S = 0, l_x = 2, l_y = 0$) have small and equal weights.

F. 1^+ resonance

Finally we address the very interesting features exhibited by the 1^+ state. We have analyzed all the characteristics of the three-body continuum [1,34] and found nearly coinciding resonances at 1.6–2.0 MeV having completely different natures. One of these strongly overlapping structures, like the 2^{+_2}, is a true three-body resonance, which is caused by a pocket in one of diagonal potentials with $K = 2, L = S = 1, l_x = l_y = 1$. Another is a coupled-channels resonance, which originates

from strong couplings in a large set of channels having repulsion in their diagonal potentials.

The intrinsic correlation plot in Fig. 11 for the 1^+ state shows a peculiar feature, namely a resonance-like behavior in the **Y** basis and a lack of it in the **T** basis. Results for the filtered $K = 2$ (Fig. 12) component shows a resonance in both bases at ~2.8 MeV with width $\Gamma \sim 1.5$ MeV in accordance with the analytic structure of the scattering amplitude. The same ridge maxima lines in both **T** and **Y** systems confirm its three-body resonance nature.

IV. CONCLUSION

We have performed a detailed study of the ^{6}He energy correlations in the Borromean three-body continuum using an $\alpha + n + n$ model with realistic interactions between the constituents, interactions that reproduce all observables in the binary subsystems. Diagnostic tools and procedures for analysis of a three-body continuum were discussed in [1,8]. In this article we have presented further developments of our continuum exploration in terms of three-body energy correlation functions.

We have discussed two main sources of amplification of continuum cross sections:

(i) true three-body resonances, which are due to interaction of *all three* constituents in the interior domain, and

(ii) a long-lived binary resonance in one of the constituent pairs

The analytic properties of (i) and (ii) and wave functions have been discussed in terms of the natural Jacobian energy correlations. They depend on the moduli of two relative momenta (energy), which are dynamic characteristics of the internal structure of excited states. These intrinsic properties of the halo excitations are manifested in the scattering amplitudes, as these characterize the asymptotics of the wave function at large distances. For sharp three-body resonances the poles in the S-matrix coincide with the peak energy, with a resonant amplification of the interior part of the wave function. The intrinsic energy correlations for 3–3 scattering should almost coincide with the transition energy correlations for reactions.

The main criterion for existence and properties of any intrinsic resonant state is that its position and other characteristics should *not* depend on the excitation mechanism (electromagnetic, strong or weak interaction). A "true" three-body resonance exists in lowest configurations, which corresponds to three particles interacting close to each other. It is partially caused by pockets in the diagonal potential terms and manifests itself by an eigenphase rapidly crossing $\pi/2$.

We have shown that the analytic properties of scattering amplitudes are displayed by outstanding structures of energy correlation functions, which for ^{6}He are most pronounced in the 2_1^+ true three-body resonance and less pronounced for the 2_2^+ and 1_1^+ resonances. In accordance with Ref. [29], it is not necessary that resonance behavior shows up in all elements of the S matrix for wide resonances. In particular the wide 2_2^+ and 1_1^+ resonances exhibit resonant behaviors only in one (2_2^+) or two (1_1^+) of the lowest partial components.

In both cases there are large contributions to the correlation function from components with higher hypermomenta K (which correspond to larger impact parameters) owing to strong coupling of different configurations, and this sometimes washes out the resonant structure. Nevertheless, filtering of the lowest configurations can reveal a three-body resonance nature, as we have shown.

In the case of a narrow resonance, the spatial wave function has strong amplification in the interior region, which corresponds to the short range of the binary interactions of all three constituents. In this situation the total resonance energy is distributed between a pair of particles and the third constituent according to the strongest binary interaction, or according to an inherent symmetry such as the Pauli principle for 2_1^+ resonance.

In addition, we have shown that there can exist "three-body virtual excitations" produced by low-lying resonances (or virtual states) in binary systems. Their pronounced inherent quality is a very long spatial range of formation, about the $n-n$ scattering length, and this leads to a very large number of configurations needed in the HH basis. There might well be a lack of deep pockets in the diagonal potential terms and strong off-diagonal (coupling) terms. Our exploration of the binary energy correlations ($n-n$ and $\alpha-n$ in ^{6}He) has shown a dominant role of the s-wave nn virtual state, and a lack of strong manifestation of the $p_{3/2}$ resonance in $\alpha-n$ (^{5}He), both for monopole and soft dipole modes. Moreover, this feature is also present in the 2^+ continuum beyond the narrow 2_1^+ resonance. The unnatural parity 1^+ excitation does not contain an s-wave nn virtual state in any component, and this generates a different shape of continuum correlations at low E_{n-n}. We will return to this issue in a separate communication. Three-body correlations for all configurations have demonstrated that, in spite of presence of a soft dipole resonance-like peak in both nuclear and electromagnetic response functions at $\sim$1.5 MeV, there is a lack of noticeable resonant behavior in the interior region (as is also true for the monopole case).

APPENDIX: MOMENTUM COORDINATES, WAVE FUNCTIONS, AND CROSS SECTIONS

We use normalized Jacobi momenta $\mathbf{k}_x$ and $\mathbf{k}_y$, which are defined in terms of laboratory momenta $\mathbf{p}_i = \hbar \mathbf{P}_i$ as

$$
\begin{aligned}
\mathbf{k}_{x3} &= (A_{12})^{-1/2}\mathbf{P}_{12} = (A_{12})^{1/2}(\mathbf{P}_2/A_2 - \mathbf{P}_1/A_1),\\
\mathbf{k}_{y3} &= (A_{(12)3})^{-1/2}\mathbf{P}_{(12)3} = (A_{(12)3})^{1/2}\\
&\quad \times [\mathbf{P}_3/A_3 - (\mathbf{P}_1+\mathbf{P}_2)/(A_1+A_2)], \quad (A1)\\
\mathbf{P} &= \mathbf{P}_1 + \mathbf{P}_2 + \mathbf{P}_3.
\end{aligned}
$$

Here $A_{12} = A_1 A_2/(A_1 + A_2)$ is the reduced mass of the $(1 + 2)$ binary subsystem (in units of the nucleon mass m), $A_{(12)3} = (A_1 + A_2)A_3/A$ is the reduced mass of the (12) pair with respect to particle 3, and $A = A_1 + A_2 + A_3$. Alternative sets, $(\mathbf{k}_{x1}, \mathbf{k}_{y1})$ and $(\mathbf{k}_{x2}, \mathbf{k}_{y2})$, of Jacobi coordinates are obtained by cyclic permutations of (1,2,3). They are connected by an orthogonal transformation (kinematic rotation)

$$
\begin{aligned}
\mathbf{k}_{xj} &= -\cos\phi_{ji}\mathbf{k}_{xi} - \sin\phi_{ji}\mathbf{k}_{yi},\\
\mathbf{k}_{yj} &= \sin\phi_{ji}\mathbf{k}_{xi} - \cos\phi_{ji}\mathbf{k}_{yi},\\
\cos\phi_{ji} &= \sqrt{\frac{A_j A_i}{A_j A_i + A_k A}}.
\end{aligned}
$$

Spatial normalized Jacobi coordinates $(\mathbf{x}_i, \mathbf{y}_i)$ are defined in an analogous way (see e.g., [1,5,6]) and have the same transformation properties. The hyperradius is given by $\rho = \sqrt{x^2 + y^2}$ in any Jacobi system, and the hyperangle in a *particular* Jacobi system (i) is defined by $\sin\alpha_i^\rho = x_i/\rho$

We shall designate the Jacobi systems of our core $+ n + n$ Borromean halo nuclei as "cluster" **T** basis with $x \sim r_{nn}$ (with corresponding $\mathbf{k}_x$) and $y \sim r_{(nn)-c}$ (with corresponding $\mathbf{k}_y$) and as "shell-model" **Y** basis (more exactly the translationally invariant shell model) with $x \sim r_{cn}$ and $y \sim r_{(cn)-n}$ coordinates. The following formulas refer to such nuclei.

The *continuum* energy E, measured from the three-body threshold, is connected with normalized Jacobi momenta via the relation $\mathbf{k}_{xi}^2 + \mathbf{k}_{yi}^2 = 2mE/\hbar^2$; that is, the invariant energy $E = \epsilon_{xi} + \epsilon_{yi}$ is partitioned into kinetic energies $\epsilon_{xi} = \hbar^2 k_{xi}^2/2m$ and $\epsilon_{yi} = \hbar^2 k_{xyi}^2/2m$ for each Jacobi subsystem, with m being the nucleonic mass. Note that the phase space volume $\sqrt{\epsilon_{xi}\epsilon_{yi}}\,d\epsilon_{xi}d\epsilon_{yi}$ is also invariant under kinematic transformations. The hypermomentum $\kappa = \sqrt{2mE/\hbar^2}$ is connected with the moduli of Jacobi momenta in a particular Jacobi system (i) via the conjugate hyperangle $\alpha_i^\kappa \in [0, \pi/2]$, which is a measure of the distribution of the total excitation energy E between the binary subsystems: $\sin\alpha_i^\kappa = k_{xi}/\kappa$, or $\sin^2\alpha_i^\kappa = \epsilon_{xi}/E$.

The bound-state and continuum wave functions can be expanded on a generalized angle-spin basis, which includes HH

$$
\mathcal{Y}_{KLM}^{l_x l_y}(\Omega_5) = \psi_K^{l_x l_y}(\alpha)\Big[Y_{l_x}(\hat{\mathbf{x}}) \otimes Y_{l_y}(\hat{\mathbf{y}})\Big]_{LM} \quad (A2)
$$

and a coupled spin function of the two halo nucleons,

$$
\begin{aligned}
X_{SM_S} &= \big[\chi_{s_1} \otimes \chi_{s_2}\big]_{SM_s}\\
&= \sum_{m_1 m_2} <s_1 m_1 s_2 m_2|SM_s> \chi_{s_1 m_1}\chi_{s_2 m_2}. \quad (A3)
\end{aligned}
$$

Here Ω_5 contains the remaining angular and hyperangular parts of the six-dimensional coordinate space $\{\mathbf{x}, \mathbf{y}\}$ ($\Omega_5^\rho = \hat{x}, \hat{y}, \alpha_\rho$) or momenta space $\{\mathbf{k_x}, \mathbf{k_y}\}$ ($\Omega_5^\kappa = \hat{k}_x, \hat{k}_y, \alpha_\kappa$), $\otimes$ is usual tensor coupling, l_x and l_y are the quantum numbers of the Jacobi orbital momenta, and L, M_L are the total orbital momentum and its projection. The hyperangular part of the HH (depending on angles α^ρ or α^κ) is defined for binary angular momenta l_x, l_y and hyperangular momentum (hypermoment) K and has the

following explicit form:

$$\psi_K^{l_x l_y}(\alpha) = N_K^{l_x l_y} (\sin \alpha)^{l_x} (\cos \alpha)^{l_y} P_{(K-l_x-l_y)/2}^{l_x+1/2, l_y+1/2}(\cos 2\alpha), \quad \text{(A4)}$$

where $P_n^{\alpha, \beta}$ are Jacobi polynomials and $N_K^{l_x l_y}$ is a normalization coefficient given by $\int \psi_K^{l_x l_y}(\alpha) \psi_{K'}^{l_x l_y}(\alpha) \sin^2 \alpha \cos^2 \alpha \, d\alpha = \delta_{KK'}$. The structure of the HH functions differs from angular spherical harmonics $Y_{l_x}(\hat{\mathbf{x}})$ or $Y_{l_y}(\hat{\mathbf{y}})$ because, as well as Jacobi polynomials (Legendre in the spherical case), they have extra $(\sin \alpha)^{l_x} (\cos \alpha)^{l_y}$ multipliers of kinematical origin. These characterize the influence of binary (Jacobi) angular momenta and hypermoment on the energy distribution.

A generalized angle-spin basis with total momentum J and projection M is constructed, by analogy with coupled-channels formulations (see, e.g., [35]), using

$$\Upsilon_{K\gamma}^{JM}(\Omega_5^\rho) = \left[\mathcal{Y}_{KL}^{l_x l_y}(\Omega_5^\rho) \otimes X_S \right]_{JM}, \quad \text{(A5)}$$

where γ refers to the quantum number set $\gamma = \{LSl_x l_y\}$ and X_{SM_S} is the channel-spin function (A3).

The antisymmetrization between two halo neutrons with definite isospin $T = 1$ can be easily done in the **T** basis, where **x** is proportional to the relative distance between two halo neutrons with definite total spin S. In the HH method, the antisymmetrizer $\hat{A}_{nn}$ acts only on the angle-spin part of scattering function and selects configurations with odd $T + S + l_x$.

The corresponding six-dimensional plane wave, with inclusion of spins s_1 and s_2 of the halo nucleons, is a reference frame for calculations of scattering amplitude and partial S-matrix elements:

$$\hat{A}_{nn} \quad (2\pi)^{-3} \exp[i(\mathbf{k_x} \cdot \mathbf{x} + \mathbf{k_y} \cdot \mathbf{y})] \cdot \chi_{s_1 m_1} \chi_{s_2 m_2}$$

$$= \hat{A}_{nn} (\kappa \rho)^{-2} \sum_{KLM_L l_x l_y} i^K J_{K+2}(\kappa \rho) \mathcal{Y}_{KLM_L}^{l_x l_y}(\Omega_5^\rho)$$

$$\times [\mathcal{Y}_{KLM_L}^{l_x l_y}(\Omega_5^\kappa)]^* \cdot \chi_{s_1 m_1} \chi_{s_2 m_2}$$

$$= \frac{\hat{A}_{nn}}{(\kappa \rho)^2} \sum_{JMK\gamma} i^K J_{K+2}(\kappa \rho)$$

$$\times \sum_{M_L M_S} \langle s_1 m_1 s_2 m_2 | SM_S \rangle \langle LM_L SM_S | JM \rangle$$

$$\times \Upsilon_{K\gamma}^{JM}(\Omega_5^\rho) \mathcal{Y}_{KLM_L}^{l_x l_y}(\Omega_5^\kappa)^*, \quad \text{(A6)}$$

where J_{K+2} is the cylindrical Bessel function of integer index.

The antisymmetrization operator $\hat{A}_{nn}$ acting on the valence nucleons in a plane wave will again select odd $T + S + l_x$. Therefore we use the term "antisymmetrised plane wave" for expression (A6).

The antisymmetrized continuum wave function in the presence of interactions between the constituents can be represented as the general solution of a coupled-channels problem for given spin projections m_1 and m_2

before collision:

$$\Psi_{m_1 m_2}^{(+)}(\mathbf{x}, \mathbf{y}, \hat{\mathbf{k}}_x, \hat{\mathbf{k}}_y, \alpha^\kappa)$$

$$= (\kappa \rho)^{-5/2} \sum_{J, K\gamma, K'\gamma'} i^K \psi_{K\gamma, K'\gamma'}^J(\kappa, \rho)$$

$$\times \Upsilon_{K'\gamma'}^{JM}(\Omega_5^\rho) \sum_{M_L M_S} \langle s_1 m_1 s_2 m_2 | SM_S \rangle$$

$$\times \langle LM_L SM_S | JM \rangle [\mathcal{Y}_{KLM_L}^{l_x l_y}(\Omega_5^\kappa)]^*, \quad \text{(A7)}$$

where $\psi_{K\gamma, K'\gamma'}^{J(+)}(\kappa \rho)$ are the ρ-radial functions. The primed indices in Eq. (A7) correspond to momenta of outgoing waves. Momenta of ingoing waves only enter the dynamical equations via the boundary conditions, such as fixed values of spin projections m_1, m_2 in the ingoing wave, as well as directions $\hat{\mathbf{k}}_x$, $\hat{\mathbf{k}}_y$ and distributions of energies α_κ of incident particles with corresponding angular l_x, l_y and hyperangular K momenta.

For hyperradial continuum wave functions, the asymptotic behavior at $\rho \to \infty$ for uncharged particles is

$$\psi_{K\gamma, K'\gamma'}^{J(+)}(\kappa \rho) = \sqrt{\frac{2}{\pi}} \frac{i}{2} \left[\mathcal{H}_{K+3/2}^-(\kappa \rho) \delta_{K\gamma, K'\gamma'} - S_{K\gamma, K'\gamma'}^J \right.$$

$$\left. \times \mathcal{H}_{K'+3/2}^+(\kappa \rho) \right]. \quad \text{(A8)}$$

Here $\mathcal{H}_{\mathcal{L}}^-$ and $\mathcal{H}_{\mathcal{L}}^+$ are the generalized well-known Riccati-Bessel functions of half-integer index, which coincide with the Coulomb functions $\mathcal{H}_{\mathcal{L}}^\pm = G_{\mathcal{L}} \pm i F_{\mathcal{L}}$ of half-integer index ($\mathcal{L} = K + 3/2$) with Sommerfeld parameter $\eta = 0$ in our case, with asymptotics $F_{K+3/2}(\kappa \rho) \simeq \sin[\kappa \rho - (K + 3/2)\pi/2]$ and $G_{K+3/2}(\kappa \rho) \simeq \cos[\kappa \rho - (K + 3/2)\pi/2]$. The functions $\mathcal{H}_{\mathcal{L}}^\pm$, having asymptotics $\sim \exp(\pm i\kappa \rho)$, describe out- and in-going three-body spherical waves, and $S_{K\gamma, K'\gamma'}^J$ is the S-matrix for the $3 \to 3$ scattering of an incoming wave Eq. (A6) in channel $K\gamma$. The factor $\sqrt{\frac{2}{\pi}} \frac{i}{2}$ gives plane wave asymptotics $J_{K+2}(\kappa \rho) \simeq \sqrt{\frac{2}{\pi \kappa \rho}} \cos[\kappa \rho - (K + 2)\pi/2 - \pi/4]$ in the absence of interaction, with normalization

$$\int \psi_{K\gamma, K'\gamma'}^{J(+)}(\kappa \rho) \psi_{K\gamma, K'\gamma'}^{J(+)}(\kappa' \rho) d\rho = \delta(\kappa - \kappa'). \quad \text{(A9)}$$

With Sommerfeld parameter $\eta = 0$, the Bessel function $J_{K+2}(\kappa \rho) = \sqrt{\frac{2}{\pi \kappa \rho}} F_{K+3/2}(\kappa \rho)$ in the whole space, so we can define the phase shift or the partial wave S matrix using $F_{K+3/2}(\kappa \rho)$ as the asymptotic form.

The factor $(\kappa \rho)^{-5/2}$ in Eq. (A7) is compensated by the behavior of the hyperradial continuum wave function $\psi_{K\gamma, K'\gamma'}^J(\kappa \rho) \sim (\kappa \rho)^{K+5/2}$ at the origin. Therefore, most important for energy dependence are the partial angular momenta of the final state, l_x, l_y ($\epsilon_x^{l_x/2} \epsilon_y^{l_y/2}$), and the polynomial structure of $P_{(K-l_x-l_y)/2}^{l_x+1/2, l_y+1/2}[(\epsilon_y - \epsilon_x)/E]$ coming from the hyperangular part of $\mathcal{Y}_{KLM_L}^{l_x l_y}(\Omega_5^\kappa)$. The lower index $n = (K - l_x - l_y)/2$ in $P_n^{l_x+1/2, l_y+1/2}$ gives the number of nodes in the polar angle $\alpha^\kappa = \text{atan}\sqrt{\epsilon_x/\epsilon_y}$ coordinate.

Since the set of hyperradial wave functions in any Jacobi system can be obtained by a linear combination of any other, we need only generate them for one Jacobi system. The

hyperharmonics $\mathcal{Y}^{l_x,l_y}_{KLM_L}$ from one Jacobi set (i) transform to another (j) via a kinematic rotation through the unitary Raynal-Revai coefficients [36]

$$\mathcal{Y}^{l_x,l_y}_{KLM_L}(\Omega^i_5) = \sum_{l'_x,l'_y} \langle j, l'_x, l'_y | i, l_x, l_y \rangle_{KL} \mathcal{Y}^{l'_x,l'_y}_{KLM_L}(\Omega^j_5). \quad \text{(A10)}$$

In this rotation the quantum numbers K, L, M are conserved. Possible values of the pairwise angular momenta l'_x, l'_y are limited by condition $(-1)^{l_x+l_y} = (-1)^{l'_x+l'_y}$ which guarantees parity conservation, and by the conservation of the hypermoment $K = 2n + l_x + l_y = 2n' + l'_x + l'_y$.

To derive the scattering amplitudes and elastic cross section it is convenient to rewrite Eq. (A7) in the matrix form

$$\Psi^{(+)}_{m_1m_2}(\mathbf{x}, \mathbf{y}, \mathbf{k}_x, \mathbf{k}_y) = \sum_{m'_1m'_2} \chi_{s_1m'_1} \chi_{s_2m'_2} \psi^{(+)}_{m'_1m'_2m_1m_2}(\mathbf{x}, \mathbf{y}, \mathbf{k}_x, \mathbf{k}_y), \tag{A11}$$

where $\psi^{(+)}_{m'_1m'_2m_1m_2}$ contains the observable spin projections $m'_1m'_2$ of the outgoing wave:

$$\psi^{(+)}_{m'_1m'_2m_1m_2}(\mathbf{x}, \mathbf{y}, \mathbf{k}_x, \mathbf{k}_y)$$
$$= (\kappa\rho)^{-5/2} \sum_{J,K\gamma,K'\gamma' M_L M_S M} \langle s_1m_1s_2m_2|SM_S\rangle\langle LM_LSM_S|JM\rangle$$
$$\times \sum_{M'_L M'_S} \langle s_1m'_1s_2m'_2|S'M'_S\rangle\langle L'M'_LS'M'_S|JM\rangle$$
$$\times i^K \mathcal{Y}^{l'_xl'_y}_{K'L'M'_L}(\Omega^\rho_5)\left[\mathcal{Y}^{l_xl_y}_{KLM_L}(\Omega^\kappa_5)\right]^* \psi^J_{K\gamma,K'\gamma'}(\kappa, \rho). \tag{A12}$$

Asymptotically the elastic scattering wave function of Eq. (A12) has the form

$$\hat{A}_{nn}(2\pi)^{-3}\exp[i(\mathbf{k}_x \cdot \mathbf{x} + \mathbf{k}_y \cdot \mathbf{y})]\delta_{m_1m'_1}\delta_{m_2m'_2}$$
$$+ f_{m'_1m'_2m_1m_2}(E, \Omega^{\kappa_f}_5, \Omega^\kappa_5)\frac{\exp(i\kappa\rho)}{\rho^{5/2}}, \tag{A13}$$

where $\rho^{-5/2}\exp(i\kappa\rho)$ is an outgoing three-body spherical wave with the antisymmetrized $3 \to 3$ scattering amplitude $f_{m'_1m'_2m_1m_2}(E, \Omega^{\kappa_f}_5, \Omega^\kappa_5)$ given at large distances ρ by

$$f_{m'_1m'_2m_1m_2}(E, \Omega^{\kappa_f}_5, \Omega^\kappa_5)$$
$$= \frac{i}{2}\sqrt{\frac{2}{\pi}}\frac{1}{\kappa^{5/2}}e^{-i\pi 3/4}$$
$$\times \sum_{JK\gamma K'\gamma'}\sum_{M_L M_S M} \langle s_1m_1s_2m_2|SM_S\rangle\langle LM_LSM_S|JM\rangle$$

$$\times \sum_{M'_L M'_S}\langle s_1m'_1s_2m'_2|S'M'_S\rangle\langle L'M'_LS'M'_S|JM\rangle$$
$$\times \left(\delta_{K\gamma;K'\gamma'} - S^J_{K\gamma;K'\gamma'}\right)\left[\mathcal{Y}^{l_xl_y}_{KLM_L}(\Omega^\kappa_5)\right]^* \mathcal{Y}^{l'_xl'_y}_{K'L'M'_L}(\Omega^{\kappa_f}_5), \tag{A14}$$

where Ω^ρ_5 is replaced by $\Omega^{\kappa_f}_5$ to characterize the directions of the momenta $\{\mathbf{k^f_x}, \mathbf{k^f_y}\}$ and energy distribution α^{κ_f} of scattered particles.

The elastic differential $3 \to 3$ scattering cross section with fixed spin projections $m'_1m'_2m_1m_2$ is defined as a square modulus of the antisymmetrized scattering amplitude:

$$\frac{d^5\sigma_{m'_1m'_2m_1m_2}(3)}{d\Omega^{\kappa_f}_5} = \left|f_{m'_1m'_2m_1m_2}(E, \Omega^{\kappa_f}_5, \Omega^\kappa_5)\right|^2. \tag{A15}$$

After averaging over the initial spin projections m_1m_2 and summing over the final $m'_1m'_2$, we have an incoherent sum over the channel spins:

$$\frac{d^5\sigma(3)}{d\Omega^{\kappa_f}_5} = \frac{1}{2\pi\kappa^5}\frac{1}{(2s_1+1)(2s_2+1)}\sum_{SM_S,S'M'_S}$$
$$\times \left|\sum_{JKLl_xl_yM_LK'L'l'_xl'_yM'_LM}\langle LM_LSM_S|JM\rangle\right.$$
$$\times \langle L'M'_LS'M'_S|JM\rangle\left(\delta_{K\gamma;K'\gamma'} - S^J_{K\gamma;K'\gamma'}\right)$$
$$\times \left.\left[\mathcal{Y}^{l_xl_y}_{KLM_L}(\Omega^\kappa_5)\right]^* \mathcal{Y}^{l'_xl'_y}_{K'L'M'_L}(\Omega^{\kappa_f}_5)\right|^2.$$

To obtain the energy correlations between scattered particles it is necessary to integrate over the directions of the incident particles and the distribution of total energy between them (Ω^κ_5), and over the direction of the scattered particles ($\hat{\mathbf{k}}^{\mathbf{f}}_{\mathbf{x}}, \hat{\mathbf{k}}^{\mathbf{f}}_{\mathbf{y}}$). After integration and summation over the projection M, the differential cross section describing the distribution of the total energy $E = \epsilon_{x_i} + \epsilon_{y_i}$ over the subsystems x_i, y_i will be an incoherent sum over the quantum numbers of the incident particles as well as the angular momenta of the scattered ones, giving the equation [Eq. (1)] we use in this paper:

$$\frac{1}{\sin^2\alpha_f\cos^2\alpha_f}\frac{d\sigma(3)}{d\alpha_f} = \frac{2}{\pi\kappa^5}\frac{1}{(2s_1+1)(2s_2+1)}$$
$$\times \sum_{JK\gamma\gamma'}(2J+1)|\sum_{K'}\left(\delta_{K\gamma;K'\gamma'}\right.$$
$$\left.- S^J_{K\gamma;K'\gamma'}\right)\psi^{l'_xl'_y}_{K'}(\alpha_f)|^2. \tag{A16}$$

---

[1] B. V. Danilin and M. V. Zhukov, Phys. At. Nucl. **56**, 460 (1993).

[2] B. V. Danilin, I. J. Thompson, J. S. Vaagen, and M. V. Zhukov, Nucl. Phys. **A632**, 383 (1998).

[3] I. J. Thompson, B. V. Danilin, V. D. Efros, J. S. Vaagen, J. M. Bang, and M. V. Zhukov Phys. Rev. C **61**, 024318 (2000).

[4] S. N. Ershov, T. Rogde, B. V. Danilin, J. S. Vaagen, I. J. Thompson, and F. A. Gareev, Phys. Rev. C **56**, 1483 (1997).

[5] M. V. Zhukov, B. V. Danilin, D. V. Fedorov, J. M. Bang, I. J. Thompson, and J. S. Vaagen, Phys. Rep. **231**, 151 (1993).

[6] B. V. Danilin, M. V. Zhukov, A. A. Korsheninnikov, L. V. Chulkov, V. D. Efros, Sov. J. Nucl. Phys. **49**, 217 (1989); **49**, 223 (1989); **53**, 71 (1991); B. V. Danilin, M. V. Zhukov,

S. N. Ershov, F. A. Gareev, R. S. Kurmanov, J. S. Vaagen, and J. M. Bang, Phys. Rev. C **43**, 2835 (1991).

[7] D. Gogny, P. Pires, and R. de Tourreil, Phys. Lett. **B32**, 591 (1970).

[8] B. V. Danilin, T. Rogde, J. S. Vaagen, I. J. Thompson, M. V. Zhukov, Phys. Rev. C **69**, 024609 (2004).

[9] B. V. Danilin, M. V. Zhukov, J. S. Vaagen, and J. M. Bang, Phys. Lett. **B302**, 129 (1993).

[10] S. N. Ershov, B. V. Danilin, T. Rogde, and J. S. Vaagen, Phys. Rev. Lett. **82**, 908 (1999).

[11] S. N. Ershov, B. V. Danilin, and J. S. Vaagen, Phys. Rev. C **64**, 064609 (2001).

[12] T. Aumann *et al.*, Phys. Rev. C **59**, 1252 (1999).

[13] L. V. Chulkov, H. Simon, I. J. Thompson *et al.*, Nucl. Phys. **A759**, 23 (2005).

[14] P. G. Hansen and B. Jonson, Europhys. Lett. **4**, 409 (1987); K. Ikeda, INS Report No. JHP-7, 1988 [in Japanese].

[15] I. J. Thompson and M. V. Zhukov, Phys. Rev. C **49**, 1904 (1994).

[16] A. C. Hayes and S. M. Sterbenz, Phys. Rev. C **52**, 2807 (1995); A. Csótó, *ibid.* **52**, 2809 (1995).

[17] A. Csótó, Phys. Lett. **B315**, 24 (1993); Phys. Rev. C **48**, 165 (1993); **49**, 2244 (1994); **49**, 3035 (1994).

[18] S. Funada, H. Kameyama, and Y. Sakuragi, Nucl. Phys. **A575**, 93 (1994).

[19] K. Arai, Y. Suzuki, and K. Varga, Phys. Rev. C **51**, 2488 (1995); K. Arai, Y. Suzuki, and R. G. Lovas, *ibid.* **59**, 1432 (1999).

[20] S. Aoyama, S. Mukai, K. Kato, and K. Ikeda, Prog. Theor. Phys. **93**, 99 (1995); **94**, 343 (1995).

[21] G. F. Filippov, K. Kato, and S. V. Korennov, Prog. Theor. Phys. **96**, 575 (1996).

[22] J. M. Bang, A. I. Mazur, A. M. Shirokov, Y. F. Smirnov, and S. A. Zaytsev, Ann. Phys. (NY) **280**, 299 (2000).

[23] A. Cobis, D. V. Fedorov, and A. S. Jensen, Phys. Rev. C **58**, 1403 (1998); E. Garrido, D. V. Fedorov, and A. S. Jensen, Nucl. Phys. **A650**, 247 (1999).

[24] B. S. Pudliner, V. R. Pandharipande, J. Carlson, S. C. Pieper, and R. B. Wiringa, Phys. Rev. C **56**, 1720 (1997); R. B. Wiringa, Nucl. Phys. **A631**, 70c (1998).

[25] T. Myo, K. Kato, S. Aoyama, and K. Ikeda, Phys. Rev. C **63**, 054313 (2001).

[26] Y. Suzuki, Nucl. Phys. **A528**, 395 (1991).

[27] G. Hagen, M. Hjorth-Jensen, and J. S. Vaagen, Phys. Rev. C **71**, 044314 (2005).

[28] S. N. Ershov, B. V. Danilin, and J. S. Vaagen, Phys. Rev. C **64**, 064609 (2001).

[29] A. M. Badalyan, L. P. Kok, M. I. Polikarpov, and Y. A. Simonov, Phys. Rep. **82**, 31 (1982).

[30] A. I. Baz', Zh. Eksp. Teor. Fiz. [Sov. Phys.—JETP] **70**, 397 (1976).

[31] V. Efimov, Comments Nucl. Part. Phys. **19**, 271 (1990).

[32] A. I. Baz' and S. P. Merkuriev, Theor. Mat. Phys. **70**, 397 (1976).

[33] In our papers [1,8] we obtained the 2_2^+ resonance at ∼2.6 MeV for a not fully converged calculatoin but the qualitative analysis is unchanged.

[34] B. V. Danilin, to be submitted.

[35] G. R. Satchler, *Direct Nuclear Reactions* (Clarendon, Oxford, 1983).

[36] J. Raynal and J. Revai, Nuovo Cimento A **68**, 612 (1970).